

**Current switching of the antiferromagnetic Néel vector in Pd/CoO/MgO(001)**M. Yang <sup>1</sup>, Q. Li,<sup>2,\*</sup> T. Wang <sup>3</sup>, B. Hong,<sup>4</sup> C. Klewe,<sup>5</sup> Z. Li,<sup>2</sup> X. Huang,<sup>6</sup> P. Shafer,<sup>5</sup> F. Zhang,<sup>4</sup> C. Hwang,<sup>7</sup> W. S. Yan,<sup>2</sup> R. Ramesh,<sup>6</sup> W. S. Zhao,<sup>4</sup> Y. Z. Wu <sup>8</sup>, Xixiang Zhang,<sup>9</sup> and Z. Q. Qiu <sup>3,†</sup><sup>1</sup>*Institute of Physical Science and Information Technology, Anhui University, Hefei, Anhui 230601, China*<sup>2</sup>*National Synchrotron Radiation Laboratory, University of Science and Technology of China, Hefei, Anhui 230029, China*<sup>3</sup>*Department of Physics, University of California, Berkeley, California 94720, USA*<sup>4</sup>*Fert Beijing Research Institute, School of Integrated Circuit Science and Engineering, Beijing Advanced Innovation Center for Big Data and Brain Computing, Beihang University, Beijing, China*<sup>5</sup>*Advanced Light Source, Lawrence Berkeley National Laboratory, Berkeley, California 94720, USA*<sup>6</sup>*Department of Materials Science and Engineering, University of California, Berkeley, California 94720, USA*<sup>7</sup>*Korea Research Institute of Standards and Science, Yuseong, Daejeon 305-340, Korea*<sup>8</sup>*Department of Physics, State Key Laboratory of Surface Physics, Fudan University, Shanghai 200433, China*<sup>9</sup>*Physical Science and Engineering Division, King Abdullah University of Science and Technology, Thuwal 23955-6900, Saudi Arabia*

(Received 12 August 2022; revised 8 October 2022; accepted 8 November 2022; published 5 December 2022)

Recently, the electrical switching of antiferromagnetic (AFM) order has been intensively investigated because of its application potential in data storage technology. Herein, we report the current switching of the AFM Néel vector in epitaxial Pd/CoO films as a function of temperature. Using combined measurements of Hall resistance (HR) and x-ray magnetic linear dichroism (XMLD) below and above the AFM Néel temperature, we unambiguously identified both magnetic and nonmagnetic contributions to the current-induced HR change. Through magnetic field-induced HR measurements, we quantitatively determined the percentage of current-induced CoO spin switching. Further, we showed that the thermal effect dominated the CoO magnetic switching more in samples with a thinner Pd layer and that samples with a thicker CoO layer required higher thermal activation for current-induced magnetic switching. These results provide a clear and comprehensive picture of current-induced AFM spin switching across the AFM Néel temperature.

DOI: [10.1103/PhysRevB.106.214405](https://doi.org/10.1103/PhysRevB.106.214405)

Antiferromagnetic (AFM) spintronics research is an emerging field in science and technology due to the numerous advantages of AFM materials over ferromagnetic (FM) materials, such as the low intrinsic damping, ultrafast spin dynamics, and the absence of stray fields [1–3]. In particular, AFM insulators (NiO or CoO) have been demonstrated to be excellent mediators of spin-current [4–8] as well as spin-torque receivers for local spin switching [9]. Notably, magnetic information technology is based on binary states, which have been traditionally written by switching FM spin orientations via an external magnetic field. The discovery of electrical switching of FM spins using spin-transfer torque [10–13] and spin-orbit torque [14–16] has offered an alternative method for writing FM bits. However, such a writing method has suffered the difficulty of a high threshold current density, which creates a severe heating effect [17]. Thus, the relatively low current density for the switching of the AFM spin axis offers a great opportunity for using AFM memory bits with electrical writing.

Most experiments on the aforementioned topic measure the magnetoresistance change as an indication of AFM spin switching (AFM-SS) between two orthogonal orientations by

applying many back-and-forth repetitions of sequential current pulses [18–22]. However, such an indirect measurement of the AFM-SS is easily mixed with other irrelevant effects (e.g., thermal effect), making it challenging to attribute the resistance change simply to the AFM-SS [23–29]. Recently, it has been demonstrated that the resistance change in experiments could entirely come from a thermal effect [30], sample morphology change [31], or thermal magnetoelastic switching [32,33]. In other words, the resistance change in an experiment could have more origins besides the AFM-SS, challenging the existence of the electrical AFM-SS.

To provide a definite answer to the AFM-SS, a direct measurement of the AFM spin orientation is needed in addition to the magnetoresistance change. In fact, x-ray linear dichroism (XLD) measurements show contrast changes after applying current pulses. However, the spatially resolved XLD results are peculiar in that only limited, submicron-size regions undergo a contrast change rather than a majority 90° AFM-SS, as suggested by the resistance measurements [9,21,34–36]. XLD measurements for biaxial AFM also show strangely intermediate contrast levels rather than the two contrast levels expected for the AFM magnetic order in two orthogonal directions. Notably, XLD effects could originate from x-ray magnetic linear dichroism (XMLD) effects that come from the AFM order as well as from the crystal field effect that is irrelevant to magnetism. In fact, an XLD effect could be dominated

\*liqian89@ustc.edu.cn

†qiu@berkeley.edu

by the crystal field effect under certain conditions, yielding a nonzero XLD signal well above the Néel temperature ( $T_N$ ), and with the XLD magnitude and even the sign depending sensitively on the crystal strains [37,38] (e.g., film thickness, growth temperature, and oxygen content [39,40]). Without careful spectroscopy analysis, it is quite easy to misinterpret the XLD contrast (e.g., photoemission electron microscopy image) change to different AFM spin orientations, particularly for the study of the electrical switching of AFM spins when the current pulse could induce local heating and hence inhomogeneous strains in a sample. Therefore, to identify clearly the presence/absence of the electrical AFM-SS, it is necessary to perform a careful and definite XMLD analysis on a well-defined system. Herein, we report a spectroscopy investigation using XMLD and a resistance investigation of the current switching of the AFM Néel vector in the Pd/CoO/MgO(001) system. We chose AFM CoO for several reasons. First, the cobalt  $L_3$  edge from CoO has a negligible crystal field effect at the normal incidence of x-rays so that the CoO  $L_3$  edge XLD signal can be well interpreted as from the CoO AFM order (e.g., the XMLD effect) [41,42]. Second, different from NiO spins, which form a spiral wall [43,44], CoO spins are locked to rotate together if the surface spin could be rotated by an external torque [45]. Therefore, the situation for NiO, where a spin rotation at the surface should twist the NiO spins into a spiral wall, should unwind itself back to the original NiO spin orientation after releasing. Hence a vanish of a  $90^\circ$  spin switching after the current pulse would not occur for CoO. Third, CoO AFM has a lower Néel temperature ( $T_N = 291$  K) than NiO ( $T_N = 525$  K), so a temperature-dependent investigation across CoO Néel temperature would easily single out the effect of the AFM order without encountering an annealing effect on the sample morphology.

A Pd(10-nm)/CoO(2.5-nm)/MgO(001) sample was prepared in an ultrahigh vacuum system using molecular beam epitaxy (MBE). The MgO(001) substrate was annealed at  $500^\circ\text{C}$ . Subsequently, a 2.5-nm CoO film was grown by evaporating cobalt at an oxygen atmosphere of  $2.0 \times 10^{-6}$  Torr. Finally, a 10-nm Pd film was deposited on the sample for current pulse application and resistance measurement. The two films were grown at RT. In the sample structure, the CoO layer was epitaxially grown with an in-plane lattice relation of CoO[110]//MgO[110] [41,42] [see the low-energy electron diffraction (LEED) patterns in Fig. 1(b)]. The sample was later fabricated into both eight- and four-terminal Hall bar structures [Fig. 1(a)] using the standard procedures of optical photolithography and the dry etching method. The Hall bar width was designed to be  $20\ \mu\text{m}$  to facilitate the XMLD measurement at beamline 4.0.2 of the advanced light source (ALS). Resistance changes were measured using the physical property measurement system.

First, we measured the current-induced resistance change and XMLD signal at RT, which is above the Néel temperature of the 2.5-nm CoO film [41], so that any resistance change would have no relation to the AFM order. The sample was made into an eight-terminal structure [Fig. 1(a)], where the writing current pulses were applied along the in-plane easy axes of CoO(001), i.e., CoO[110] ( $x$ -axis) and CoO[1 $\bar{1}$ 0] ( $y$ -axis) directions. For the electrical detection of the AFM Néel vector orientation, a constant reading current was applied

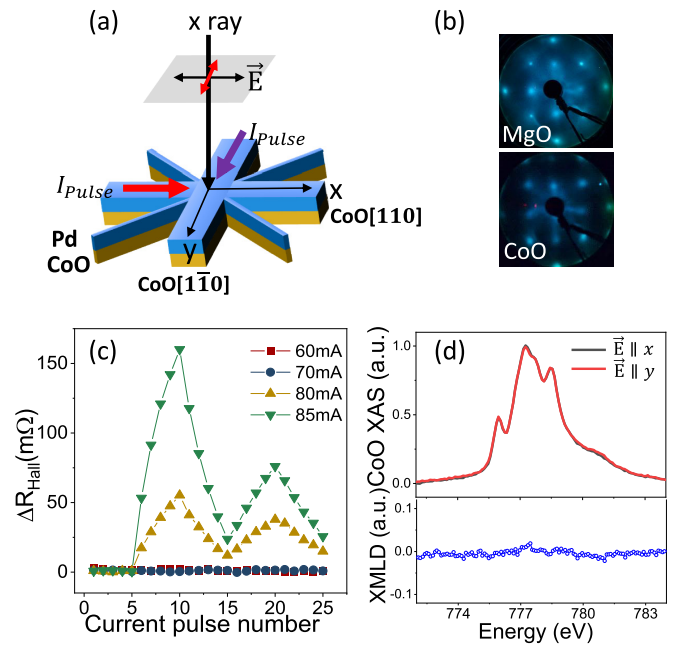


FIG. 1. (a) A schematic of current switching and XMLD measurements on the eight-terminal Hall bar structure of the Pd(10-nm)/CoO(2.5-nm)/MgO(001) sample. The width is  $20\ \mu\text{m}$  for the writing pulse current path along the easy magnetization axes of CoO[110] ( $x$ -axis) and CoO[1 $\bar{1}$ 0] ( $y$ -axis), and  $5\ \mu\text{m}$  for the reading current (1 mA) path along the diagonal directions. (b) LEED patterns of the CoO film and MgO(001) substrate. (c) The HR change as a function of the current pulse number. The direction of the current pulse changes after every five pulses, as depicted by the red and purple arrows in (a). (d) CoO spectra measured with linear polarization of the x-ray parallel and perpendicular to the  $x$ -axis, and the corresponding XMLD between the two polarizations. All measurements were performed at RT, which is higher than the CoO Néel temperature.

along the  $[0\bar{1}0]$  direction and the Hall voltage was measured at the orthogonal  $[100]$  direction. This transverse spin magnetoresistance [or in-plane spin Hall resistance (HR)] was recorded to indicate the CoO spin switching, where CoO spins parallel to  $[1\bar{1}0]$  and  $[110]$  yielded the maximum and minimum HRs, respectively [18–32]. In the current-induced resistance change measurement [Fig. 1(c)], we applied zero current pulses for the first five points, a 10-ms-long current pulse along the  $x$ -axis (red arrow) for the subsequent five points, and then along the  $y$ -axis (purple arrow) for the following next five points [Fig. 1(a)]. The writing current pulse direction was switched back and forth every five points. The HR,  $\Delta R_{\text{Hall}}$ , showed a sawtooth-like signal at large current pulses of 80 mA ( $j = 4.0 \times 10^{11}\ \text{A}\cdot\text{m}^{-2}$ ) and 85 mA ( $j = 4.25 \times 10^{11}\ \text{A}\cdot\text{m}^{-2}$ ). For the current pulse number dependent electrical measurements, we removed an offset from the original data to make all data of HR change at different writing current pulses starting from zero. To confirm the absence of the CoO magnetic order, an XMLD measurement [Fig. 1(d)] was performed with a linearly polarized x-ray spot focused on the center of the Hall bar structure. X-ray absorption spectra (XAS) show an identical shape for x-rays with the linear polarization along the  $x$ - and  $y$ -axes. Correspondingly, the

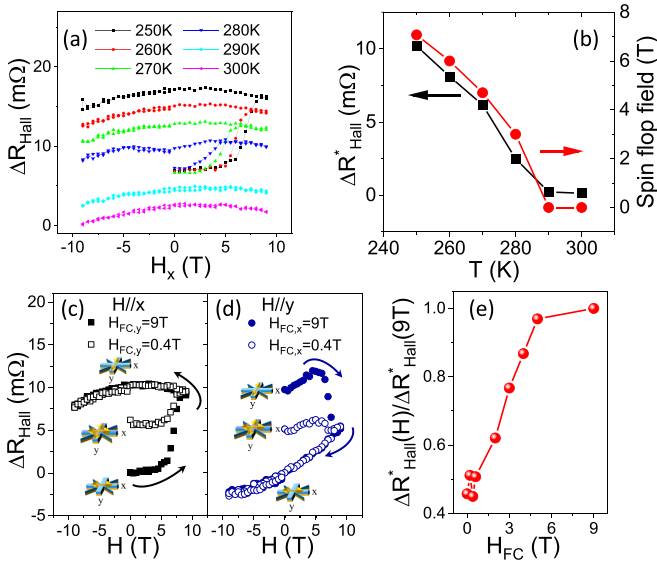


FIG. 2. (a) HR as a function of increasing  $H_x$  after field cooling (FC) with  $H_{FC,y} = 9$  T at various temperatures across the CoO Néel temperature. (b) HR change and spin flop field as a function of temperature extracted from (a). HR change as a function of increasing  $H_x$  (or  $H_y$ ) after FC with (c)  $H_{FC,y} = 0.4$  T or 9 T, or (d)  $H_{FC,x} = 0.4$  T or 9 T. (e) HR change during field scanning normalized with  $\Delta R_{\text{Hall}}$  using a FC of 9 T as a function of FC strength. Field-dependent measurements in (c) and (d) were performed at 250 K.

difference between the spectra at the two polarizations (XMLD signals) is zero at the cobalt edge, showing the paramagnetic state of the CoO layer at RT. Therefore, the result unambiguously demonstrates that the sawtooth-like HR change in Fig. 1(c) arises from a nonmagnetic origin.

We investigated the dependence of the HR on temperature and field cooling (FC) strength. After FC within  $H_{FC} = 9$  T along the  $y$ -axis, we applied a scanning field along the  $x$ -axis at various temperatures [Fig. 2(a)]. The HR exhibits a jump with increasing FC strength of  $H_x$ . Such a jump can be attributed to the switching of the CoO Néel vector, where the middle value of the HR jump is defined as the spin flop field of CoO [27]. Figure 2(b) shows that both the HR change ( $\Delta R_{\text{Hall}}^*$ , defined as the difference between the value of  $\Delta R_{\text{Hall}}$  at 0 T after CoO spin switching and the initial value of  $\Delta R_{\text{Hall}}$  at 0 T) and the spin flop field decrease with increasing temperature and vanish above 290 K, indicating a Néel temperature of  $\sim 290$  K in our CoO film. We also found that the CoO domain state at low temperatures is closely related to the FC strength. For FC at  $H_{FC} = 0.4$  T, the field-dependent HR change  $\Delta R_{\text{Hall}}^*$  was roughly  $\sim 50\%$  of that for FC at  $H_{FC} = 9$  T [Figs. 2(c) and 2(d)]. The opposite trend of field-dependent  $\Delta R_{\text{Hall}}$  can be understood as the CoO spin switching in a magnetic field along the [110] or  $[1\bar{1}0]$  direction [Figs. 2(c) and 2(d)]. The summarized HR change  $\Delta R_{\text{Hall}}^*(H)/\Delta R_{\text{Hall}}^*(9\text{ T})$  as a function of the FC strength remains at  $\sim 0.5$  below a 0.6-T cooling field, and saturates at  $\sim 1$  for  $H_{FC}$  above 5 T [Fig. 2(e)]. This result suggests that CoO is magnetized into a single domain at a low temperature only for  $H_{FC}$  above 5 T and should be in a multidomain

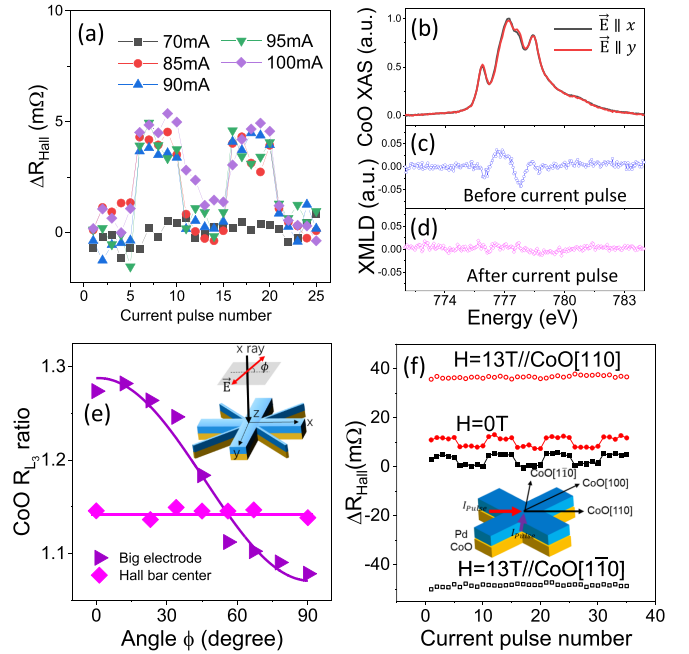


FIG. 3. (a) HR change as a function of the current pulse number. The direction of the current pulse changes after every five pulses, as depicted by the red and purple arrows in Fig. 1(a). (b) CoO spectra measured with linear polarization of the x-ray parallel to the CoO[110] and CoO[ $1\bar{1}0$ ] directions. The corresponding XMLD (c) before and (d) after the current pulse along the CoO[110] (the  $x$ -axis). (e) X-ray polarization angle  $\phi$  dependence of the CoO  $R_{L3}$  ratio collected from both the big electrode and the Hall bar center. (f) The HR change in a four-terminal Hall bar structure as a function of current pulse number with  $H = 13$  T applied along the CoO[110] direction (hollow symbols) and  $H = 0$  T (solid symbols). All measurements were performed at 200 K.

state with  $\sim 50\%$  aligned along CoO[110] and  $\sim 50\%$  aligned along CoO[ $1\bar{1}0$ ] for FC below 0.6 T.

Next, we performed the measurement of current-induced AFM order switching at 200 K, which is below the CoO Néel temperature. The sample was cooled down from 320 to 200 K within a 9-T FC along the  $y$ -axis ( $H_{FC,y} = 9$  T). Different from the sawtooth-like HR change above the Néel temperature [Fig. 1(c)], the HR change in this case [Fig. 3(a)] shows a step-like signal at current pulses ranging between 85 mA ( $j = 4.25 \times 10^{11}$  A·m $^{-2}$ ) and 100 mA ( $j = 5.0 \times 10^{11}$  A·m $^{-2}$ ) of the writing current pulse. To confirm whether the step-like change of the electrical signal comes from the magnetic origin, we performed XMLD measurements [Fig. 3(b)] both before [Fig. 3(c)] and after [Fig. 3(d)] the application of five writing current pulses at 100 mA ( $j = 5.0 \times 10^{11}$  A·m $^{-2}$ ). The XMLD signals showed a dramatic change after applying the current pulses. Considering that the current pulses could cause intense heat in the Hall bar structure [30], inducing a possible change in the XMLD signal within the heat dissipation time, we performed XMLD measurements 8 h after applying current pulses. The XMLD result remains the same as the signal in Fig. 3(d), suggesting that heating is not responsible for the change in the XMLD signal after applying the current pulses. The x-ray spot size is about 100  $\mu\text{m}$

(horizontal)  $\times 50 \mu\text{m}$  (vertical). Although the x-ray collects an overall signal below the spot size, the majority of the signal comes from the area of current-induced switching for current pulses along the  $x$ -axis (writing path along the  $x$ -axis).

For quantitative analysis, CoO XAS were measured using linearly polarized x-rays, with the linear polarization changing from  $\phi = 0^\circ$  to  $90^\circ$ , where  $\phi$  is defined as the angle between the x-ray polarization and the  $x$ -axis [Fig. 3(e)]. The CoO  $R_{L3}$  ratio, which represents the maximum difference of the XMLD signal, is defined as the intensity of the XAS at an energy of 777.2 eV over the intensity at an energy of 777.6 eV. The CoO  $R_{L3}$  ratio at a big electrode exhibits a clear quadratic dependence on sinusoidal  $\phi$  and can be well-fitted by  $R_{L3}(\phi) = A\cos^2(\phi - \phi_0) + B$  [41,44]. Both the CoO  $R_{L3}(\phi)$  at the big electrode [Fig. 3(e)] and the XMLD signal at the Hall bar center before the application of the current pulse [Fig. 3(c)] suggest that more CoO Néel vectors are along CoO[110] ( $x$ -axis). Contrary to the clear  $\phi$  dependence of the CoO  $R_{L3}$  ratio in the big electrode, the Hall bar center after applying current pulses as a function of  $\phi$  shows an almost constant behavior, indicating the multidomain state of CoO with an equal number of spins aligning along the CoO[110] ( $x$ -axis) and CoO[1 $\bar{1}$ 0] ( $y$ -axis) directions [44]. Notably, the CoO sample in the XMLD measurement was cooled within  $H_{FC,y} = 0.4 \text{ T}$ —the highest magnetic field available at BL4.0.2 of ALS. From the HR measurement results on the same sample, a cooling field below 0.6 T should yield an approximately equal number of CoO domains with Néel vectors in the [110] and [1 $\bar{1}$ 0] directions. We notice the fact that even though the big electrode shows a clear cosine square change, the change of the CoO  $R_{L3}$  ratio (an amplitude of  $\sim 0.2$ ) is still less than the full amplitude ( $\sim 0.43$ ) from single-domain CoO layer [8]. Another technical detail in the XMLD measurement is that the XMLD magnitude depends sensitively on the MgO substrate treatment, possibly caused by atomic terrace details, defects, local strains, etc. Subsequently, the XMLD results [Fig. 3(f)] clearly demonstrate the magnetic origin of the step-like HR change, i.e., the pulse current prefers to align the CoO Néel vectors to the orthogonal direction, and the application of 100-mA current pulses along the  $x$ -axis at 200 K induces a partial switching of the CoO Néel vectors from the  $x$ -axis to the  $y$ -axis, which agrees with a previous study on the current-induced switching of CoO at low temperatures [27]. Although bulk CoO contains spins orthogonal to the (001) plane, it has been demonstrated that epitaxial CoO(001) thin films grown on MgO(001) substrate should have in-plane-oriented spins [46,47]. Both the transport and XMLD measurements were set to probe the in-plane  $90^\circ$  switching of CoO spins. In addition, because AFM spins have only a spin axis rather than a direction, XMLD measurement cannot discern out-of-plane AFM spin switching (e.g., a  $180^\circ$  switching of both AFM sublattice spins gives the same XMLD signal).

To verify further the magnetic origin of the current-induced HR, we also performed the HR measurement in a four-terminal Hall bar structure. The sample showed a step-like HR change after applying a current pulse of  $j = 4.0 \times 10^{11} \text{ A}\cdot\text{m}^{-2}$  along the [110] or [1 $\bar{1}$ 0] direction, and alternating every five points in the absence of a magnetic field. Conversely,  $\Delta R_{\text{Hall}}$  exhibits a negligible change as a function of the current pulse number within a strong magnetic field of 13 T for both the

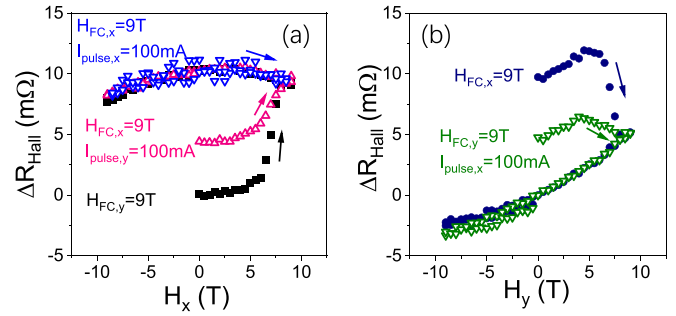


FIG. 4. (a) HR change as a function of increasing  $H_x$  after FC ( $H_{FC,y} = 9\text{ T}$ ) and ( $H_{FC,x} = 9\text{ T}$ ) plus a current pulse applied along the  $y$ -axis ( $I_{\text{pulse},y} = 100\text{ mA}$ ) and the  $x$ -axis ( $I_{\text{pulse},x} = 100\text{ mA}$ ), respectively. (b) HR change as a function of increasing  $H_y$  after FC ( $H_{FC,x} = 9\text{ T}$ ) and ( $H_{FC,y} = 9\text{ T}$ ) plus a current pulse applied along the  $y$ -axis ( $I_{\text{pulse},y} = 100\text{ mA}$ ). All measurements were performed at 250 K.

$H//$ [110] and [1 $\bar{1}$ 0] directions, further confirming the magnetic origin of the step-like resistance change, because the 13-T field strength is sufficiently strong to align the CoO into a single-domain state. Therefore, the difference in the HR between  $H//$ [110] and [1 $\bar{1}$ 0] should correspond to a complete switching of the CoO spins. From the amplitude of  $\Delta R_{\text{Hall}}$  change, we estimate that the step-like  $\Delta R_{\text{Hall}}$  at a current pulse of  $j = 4.0 \times 10^{11} \text{ A}\cdot\text{m}^{-2}$  corresponds to only  $\sim 5\%$  switching of CoO spins.

The percentage of current-induced CoO spin switching was also investigated by combining the current- and field-induced CoO spin switching. First, we aligned CoO into a single domain with  $H_{FC,x} = 9\text{ T}$  [Fig. 4(a)] or  $H_{FC,y} = 9\text{ T}$  [Fig. 4(b)]. Subsequently, a current pulse of 100 mA ( $j = 5.0 \times 10^{11} \text{ A}\cdot\text{m}^{-2}$ ) was applied perpendicular to the field direction at 250 K. Finally,  $\Delta R_{\text{Hall}}$  was measured under the sweeping field of  $H_x$  [Fig. 4(a)] or  $H_y$  [Fig. 4(b)], where CoO spins could fully rotate to the direction orthogonal to the magnetic field direction. Under these conditions, only the CoO spins (spin along the  $x$ -axis or  $y$ -axis) switched by the current pulse contributed to the  $\Delta R_{\text{Hall}}$  change, so that the efficiency of CoO spin switching could be obtained by comparing the  $\Delta R_{\text{Hall}}$  amplitude to that from single CoO domain switching in Fig. 4(a) or Fig. 4(b). Using a current pulse of  $5.0 \times 10^{11} \text{ A}\cdot\text{m}^{-2}$  at 250 K, we found that the efficiency of current-induced switching was  $\sim 57.3\%$  and  $\sim 49.0\%$ , respectively, for the CoO spins from the [110] to [1 $\bar{1}$ 0] and the [1 $\bar{1}$ 0] to [110] directions. One may argue that whether the observed resistance differences between two curves in both Figs. 4(a) and 4(b) is due to the intense heat generated by the current pulses, so that the temperature was enhanced to above the Néel temperature and then a multidomain state (50% CoO spins along [110] and 50% CoO spins along [1 $\bar{1}$ 0]) was created after cooling down. An additional experiment was performed with  $H_{FC,x} = 9\text{ T}$  and  $I_{\text{pulse},y} = 100\text{ mA}$ , where the current pulse was applied parallel to the cooling field direction and should also yield the multidomain state of CoO considering the thermal origin. However, we found an almost flat line, with resistance fluctuating around  $10 \text{ m}\Omega$  [Fig. 4(a)], demonstrating the magnetic origin of current-induced

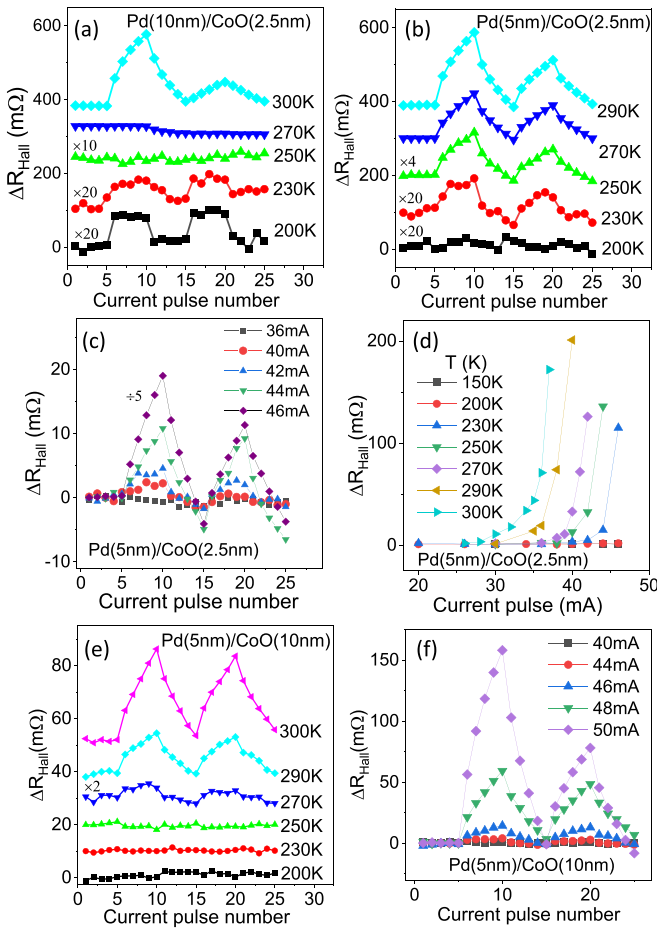


FIG. 5. (a) Current pulse-induced HR changes at 90 mA for 200, 230, 250, and 270 K, and at 85 mA for 300 K from a Pd(10-nm)/CoO(2.5-nm) sample. (b) Current pulse-induced HR change at 42 mA for 200, 230, 250, and 270 K, and at 40 mA for 290 K from a Pd(5-nm)/CoO(2.5-nm) sample. (c) Selected  $\Delta R_{\text{Hall}}$  signal as a function of current pulse number at 230 K from the Pd(5-nm)/CoO(2.5-nm) sample. (d) Summary of the  $\Delta R_{\text{Hall}}$  amplitude as a function of current pulse density at various temperatures from the Pd(5-nm)/CoO(2.5-nm) sample. (e) Current pulse-induced HR change at 46 mA for 200, 230, 250, 270, and 290 K, and at 45 mA for 300 K from a Pd(5-nm)/CoO(10-nm) sample. (f) Selected  $\Delta R_{\text{Hall}}$  signal as a function of current pulse number from the Pd(5-nm)/CoO(10-nm) sample at 290 K. The Hall bar width of the writing current pulse is 20  $\mu\text{m}$  for all panels.

switching in antiferromagnets instead of the previously speculated thermal origin.

To reveal the crossover of  $\Delta R_{\text{Hall}}$  from the magnetic originated step-like shape at low temperatures [Fig. 3(a)] to the nonmagnetic originated saw-like shape above the Néel temperature [Fig. 1(c)], we performed the current pulse switching measurement at different temperatures across the CoO Néel temperature.  $\Delta R_{\text{Hall}}$  at a current pulse density of  $j = 4.5 \times 10^{11} \text{ A}\cdot\text{m}^{-2}$  shows a step-like behavior at 200 K and evolves into a sawtooth-like behavior at 300 K [Fig. 5(a)]. Recalling that  $\Delta R_{\text{Hall}}$  due to CoO spin switching diminishes at a temperature higher than  $T_N \sim 290 \text{ K}$  [Fig. 2(b)], the total current-induced  $\Delta R_{\text{Hall}}$  shown in Fig. 5(a) clearly

shows a crossover from the magnetic origin to the nonmagnetic origin with increasing temperature. The amplitude of step-like  $\Delta R_{\text{Hall}}$  decreases gradually as the temperature increases toward CoO Néel temperature due to the reduced CoO AFM order and subsequently evolves into the sawtooth-like shape as the temperature increases to 300 K (above  $T_N$ ). The sawtooth-like signal change exhibits a clear, enhanced magnitude compared with the step-like signal change, suggesting a Joule heating origin, which has been addressed in the literature [21,25]. Because the heating effect should be present at all temperatures, although less severe at lower temperatures, we further investigated  $\Delta R_{\text{Hall}}$  behaviors in a thinner lead film in which the heating effect should be enhanced at the same current density. We prepared another sample of Pd(5 nm)/CoO(2.5 nm) with a thinner lead layer and performed the current switching HR measurement at a similar current pulse density [ $j = 4.2 \times 10^{11} \text{ A}\cdot\text{m}^{-2}$ ; Fig. 5(b)].  $\Delta R_{\text{Hall}}$  changes from an approximate step-like shape at 230 K to a sawtooth-like shape at 250 K. Noting that 250 K is below the CoO Néel temperature, this result demonstrates that the HR change comes from a mixture of the two effects, and the thermal effect is indeed present at all temperatures and starts to outweigh the spin-orbit torque effect in the Pd(5-nm)/CoO(2.5-nm) sample at a temperature near but below the Néel temperature.

The different behaviors of  $\Delta R_{\text{Hall}}$  in the two samples are also reflected in  $\Delta R_{\text{Hall}}$  at different current pulse densities [Fig. 5(c)]. We found that the HR in the Pd(5-nm)/CoO(2.5-nm) lead sample remained almost flat at a current pulse of 36 mA, changed to a step-like shape at 40 mA, and changed to a sawtooth-like shape with a further increase of the current pulse amplitude, which is similar to the current-switching behavior in other systems, such as NiO [21,28] and  $\alpha\text{-Fe}_2\text{O}_3$  [25]. The  $\Delta R_{\text{Hall}}$  amplitude increases at a high current density in the Pd(5-nm)/CoO(2.5-nm) lead sample, different from the result in the 10-nm lead sample [Fig. 3(a)]. Figure 5(d) summarizes the extracted  $\Delta R_{\text{Hall}}$  amplitudes (defined as the maximum resistance change after applying five current pulses) at different temperatures. The  $\Delta R_{\text{Hall}}$  amplitude exhibits zero value at a low current density and increases sharply above a threshold at higher current densities to exhibit the characteristic step-like shape from the CoO spin switching. The existence of the current density threshold suggests the existence of an energy barrier for the electrical switching of CoO spins. We found that the current-density threshold value decreases with increasing temperature, thereby offering an opportunity to investigate the influence of the ambient temperature on the electrical switching of CoO spins.

Further, we investigated the influence of CoO thickness on a current-induced  $\Delta R_{\text{Hall}}$  change. Hence, we prepared another sample with a 10-nm CoO film. For the Pd(5-nm)/CoO(10-nm) sample [Fig. 5(e)],  $\Delta R_{\text{Hall}}$  remains almost constant at low temperatures, exhibits an approximate step-like shape at 270 K, and gradually changes to a sawtooth-like shape at 300 K. Our previous study [42] showed that the energy barrier for CoO spin switching increased linearly with CoO thickness; therefore, a current pulse of 46 mA would be insufficient to switch the spins in the 10-nm CoO film at low temperatures.

The required higher ambient temperature of a sizable current-induced  $\Delta R_{\text{Hall}}$  signal for the Pd(5-nm)/CoO(10-nm) sample is consistent with the physical picture of the rigid rotation of the entire CoO spins in the experiment. From Fig. 5(f), the current density to switch CoO Néel vectors or to generate a sizable  $\Delta R_{\text{Hall}}$  signal in the Pd(5-nm)/CoO(10-nm) sample is obviously greater than that in the Pd(5-nm)/CoO(5-nm) sample, demonstrating a greater energy barrier for CoO spin switching with a thicker CoO layer.

There are multiple efficiencies of current-induced switching in this experiment. The different current-induced switching efficiencies could be attributed to different temperatures, current densities, samples structures, etc. Our previous study [42] showed CoO spin-switching probability exponentially increases with temperature following the Arrhenius law. Thus, it is expected to have a low spin-switching efficiency at low temperature and a much higher current-switching efficiency at higher temperature. Although the heavy metal in the Pd/CoO system is not the best material for inducing spin-current torque [48], lead is also a heavy metal with strong spin-orbit interaction, and can be grown by a thermal evaporator. Thus, a good quality of interface was guaranteed in the MBE chamber. Our result of a current-induced step-like HR change and XMLD signal, which remains the same even 8 h after applying the current pulses, suggests heating is not responsible for the change of the XMLD signal at low temperature. Our result extends the topic of current-induced spin switching in antiferromagnets to heavy metal (HM)/AFM systems, with the HM possessing small spin-charge conversion efficiency (such as lead).

In summary, we investigated the current-induced switching of the AFM Néel vector in the Pd/CoO/MgO(001) system across the CoO Néel temperature. Combining HR and XMLD measurements, we unambiguously identified two different

origins of HR change after electrical current pulses were applied: a sawtooth-like signal at a temperature above the Néel temperature from a nonmagnetic thermal effect and a step-like signal at a temperature below the Néel temperature from the CoO Néel vector switching, with the percentage of CoO spin switching depending on the current density, FC strength, and lead-capping and CoO-AFM layer thicknesses. Our findings reveal a clear and comprehensive relationship between the current-induced HR change and the AFM Néel order switching in HM/AFM systems and highlight new device potentials in AFM spintronics.

This work was supported by the National Natural Science Foundation of China (Grants No. 12104003, No. 12174364, No. 11734006, and No. 11974079), the Users with Excellence Program of Hefei Science Center CAS (Grant No. 2021HSC-UE003), the Natural Science Foundation of Anhui Province (Grant No. 2108085QA20), the Fundamental Research Funds for the Central Universities (No. wk2310000104), and the Open Fund of the State Key Laboratory of Surface Physics of Fudan University (Grant No. KF2020\_06 and KF2021\_05). This work was also supported by the U.S. Department of Energy, Office of Science, Office of Basic Energy Sciences, Materials Sciences and Engineering Division under Contract No. DE-AC02-05-CH11231 (van der Waals heterostructures program, KCWF16). This research used resources of the Advanced Light Source, which is a DOE Office of Science User Facility under Contract No. DE-AC02-05CH11231 and Beamlines MCD-A and MCD-B (Soochow Beamline for Energy Materials) at NSRL. The nanofabrication in this work was carried out at the USTC Center for Micro and Nanoscale Research and Fabrication. This publication is based upon work supported by King Abdullah University of Science and Technology under Award No. ORA-CRG10-2021-4665.

- 
- [1] T. Jungwirth, X. Marti, P. Wadley, and J. Wunderlich, *Nat. Nanotech.* **11**, 231 (2016).
- [2] M. B. Jungfleisch, W. Zhang, and A. Hoffmann, *Phys. Lett. A* **382**, 865 (2018).
- [3] V. Baltz, A. Manchon, M. Tsoi, T. Moriyama, T. Ono, and Y. Tserkovnyak, *Rev. Mod. Phys.* **90**, 015005 (2018).
- [4] H. Wang, C. Du, P. C. Hammel, and F. Yang, *Phys. Rev. Lett.* **113**, 097202 (2014).
- [5] C. Hahn, G. D. Loubens, V. V. Naletov, J. B. Youssef, O. Klein, and M. Viret, *Europhys. Lett.* **108**, 57005 (2014).
- [6] W. Lin, K. Chen, S. Zhang, and C. L. Chien, *Phys. Rev. Lett.* **116**, 186601 (2016).
- [7] Z. Qiu, J. Li, D. Hou, E. Arenholz, A. T. N'Diaye, A. Tan, K. Uchida, K. Sato, S. Okamoto, Y. Tserkovnyak, Z. Q. Qiu, and E. Saitoh, *Nat. Commun.* **7**, 12670 (2016).
- [8] Q. Li, M. Yang, C. Klewe, P. Shafer, A. T. N'Diaye, D. Hou, T. Y. Wang, N. Gao, E. Saitoh, C. Hwang, R. J. Hicken, J. Li, E. Arenholz, and Z. Q. Qiu, *Nat. Commun.* **10**, 5265 (2019).
- [9] P. Wadley *et al.*, *Science* **351**, 587 (2016).
- [10] J. C. Slonczewski, *J. Magn. Magn. Mater.* **159**, L1 (1996).
- [11] L. Berger, *Phys. Rev. B* **54**, 9353 (1996).
- [12] M. Tsoi, A. G. M. Jansen, J. Bass, W.-C. Chiang, M. Seck, V. Tsoi, and P. Wyder, *Phys. Rev. Lett.* **80**, 4281 (1998).
- [13] E. B. Myers, D. C. Ralph, J. A. Katine, R. N. Louie, and R. A. Buhrman, *Science* **285**, 867 (1999).
- [14] I. M. Miron, K. Garello, G. Gaudin, P. J. Zermatten, M. V. Costache, S. Auffret, S. Bandiera, B. Rodmacq, A. Schuhl, and P. Gambardella, *Nature (London)* **476**, 189 (2011).
- [15] L. Liu, C. F. Pai, Y. Li, H. W. Tseng, D. C. Ralph, and R. A. Buhrman, *Science* **336**, 555 (2012).
- [16] L. Liu, O. J. Lee, T. J. Gudmundsen, D. C. Ralph, and R. A. Buhrman, *Phys. Rev. Lett.* **109**, 096602 (2012).
- [17] T. Kawahara, K. Ito, R. Takemura, and H. Ohno, *Microelectron. Reliab.* **52**, 613 (2012).
- [18] K. Olejnik, V. Schuler, X. Marti, V. Nova, Z. Kaspar, P. Wadley, R. P. Campion, K. W. Edmonds, B. L. Gallagher, J. Garces, M. Baumgartner, P. Gambardella, and T. Jungwirth, *Nat. Commun.* **8**, 15434 (2017).
- [19] S. Y. Bodnar, L. Šmejkal, I. Turek, T. Jungwirth, O. Gomonay, J. Sinova, A. A. Sapozhnik, H.-J. Elmers, M. Kläui, and M. Jourdan, *Nat. Commun.* **9**, 348 (2018).
- [20] X. Z. Chen, R. Zarzuela, J. Zhang, C. Song, X. F. Zhou, G. Y. Shi, F. Li, H. A. Zhou, W. J. Jiang, F. Pan, and Y. Tserkovnyak, *Phys. Rev. Lett.* **120**, 207204 (2018).
- [21] L. Baldtrati, O. Gomonay, A. Ross, M. Filianina, R. Lebrun, R. Ramos, C. Leveille, F. Fuhrmann, T. R. Forrest, F. Maccherozzi,

- S. Valencia, F. Kronast, E. Saitoh, J. Sinova, and M. Kläui, *Phys. Rev. Lett.* **123**, 177201 (2019).
- [22] I. Gray, T. Moriyama, N. Sivadas, G. M. Stiehl, J. T. Heron, R. Need, B. J. Kirby, D. H. Low, K. C. Nowack, D. G. Schlom, D. C. Ralph, T. Ono, and G. D. Fuchs, *Phys. Rev. X* **9**, 041016 (2019).
- [23] M. Meinert, D. Graulich, and T. Matalla-Wagner, *Phys. Rev. Applied* **9**, 064040 (2018).
- [24] P. Zhang, J. Finley, T. Safi, and L. Liu, *Phys. Rev. Lett.* **123**, 247206 (2019).
- [25] Y. Cheng, S. Yu, M. Zhu, J. Hwang, and F. Yang, *Phys. Rev. Lett.* **124**, 027202 (2020).
- [26] T. Matalla-Wagner, J.-M. Schmalhorst, G. Reiss, N. Tamura, and M. Meinert, *Phys. Rev. Res.* **2**, 033077 (2020).
- [27] L. Baldrati, C. Schmitt, O. Gomonay, R. Lebrun, R. Ramos, E. Saitoh, J. Sinova, and M. Kläui, *Phys. Rev. Lett.* **125**, 077201 (2020).
- [28] F. Schreiber, L. Baldrati, C. Schmitt, R. Ramos, E. Saitoh, R. Lebrun, and M. Kläui, *Appl. Phys. Lett.* **117**, 082401 (2020).
- [29] E. Cogulu, N. N. Statuto, Y. Cheng, F. Yang, R. V. Chopdekar, H. Ohldag, and A. D. Kent, *Phys. Rev. B* **103**, L100405 (2021).
- [30] C. C. Chiang, S. Y. Huang, D. Qu, P. H. Wu, and C. L. Chien, *Phys. Rev. Lett.* **123**, 227203 (2019).
- [31] A. Churikova, D. Bono, B. Neltner, A. Wittmann, L. Scipioni, A. Shepard, T. Newhouse-Illige, J. Greer, and G. S. D. Beach, *Appl. Phys. Lett.* **116**, 022410 (2020).
- [32] H. Meer, F. Schreiber, C. Schmitt, R. Ramos, E. Saitoh, O. Gomonay, J. Sinova, L. Baldrati, and M. Kläui, *Nano Lett.* **21**, 114 (2021).
- [33] C. Schmitt, L. Baldrati, L. Sanchez-Tejerina, F. Schreiber, A. Ross, M. Filianina, S. Ding, F. Fuhrmann, R. Ramos, F. Maccherozzi, D. Backes, M.- A. Mawass, F. Kronast, S. Valencia, E. Saitoh, G. Finocchio, and M. Kläui, *Phys. Rev. Appl.* **15**, 034047 (2021).
- [34] M. J. Grzybowski, P. Wadley, K. W. Edmonds, R. Beardsley, V. Hills, R. P. Campion, B. L. Gallagher, J. S. Chauhan, V. Novak, T. Jungwirth, F. Maccherozzi, and S. S. Dhesi, *Phys. Rev. Lett.* **118**, 057701 (2017).
- [35] P. Wadley, S. Reimers, M. J. Grzybowski, C. Andrews, M. Wang, J. S. Chauhan, B. L. Gallagher, R. P. Campion, K. W. Edmonds, S. S. Dhesi, F. Maccherozzi, V. Novak, J. Wunderlich, and T. Jungwirth, *Nat. Nanotechnol.* **13**, 362 (2018).
- [36] T. Moriyama, K. Oda, T. Ohkochi, M. Kimata, and T. Ono, *Sci. Rep.* **8**, 141167 (2018).
- [37] S. Altieri, M. Finazzi, H. H. Hsieh, H.-J. Lin, C. T. Chen, T. Hibma, S. Valeri, and G. A. Sawatzky, *Phys. Rev. Lett.* **91**, 137201 (2003).
- [38] M. W. Haverkort, S. I. Csiszar, Z. Hu, S. Altieri, A. Tanaka, H. H. Hsieh, H.-J. Lin, C. T. Chen, T. Hibma, and L. H. Tjeng, *Phys. Rev. B* **69**, 020408(R) (2004).
- [39] Y. Z. Wu, Y. Zhao, E. Arenholz, A. T. Young, B. Sinkovic, C. Won, and Z. Q. Qiu, *Phys. Rev. B* **78**, 064413 (2008).
- [40] Y. Z. Wu, B. Sinkovic, C. Won, J. Zhu, Y. Zhao, and Z. Q. Qiu, *Phys. Rev. B* **85**, 134436 (2012).
- [41] Q. Li, T. Gu, J. Zhu, Z. Ding, J. X. Li, J. H. Liang, Y. M. Luo, Z. Hu, C. Y. Hua, H.-J. Lin, T. W. Pi, C. Won, and Y. Z. Wu, *Phys. Rev. B* **91**, 104424 (2015).
- [42] Q. Li, G. Chen, T. P. Ma, J. Zhu, A. T. N'Diaye, L. Sun, T. Gu, Y. Huo, J. H. Liang, R. W. Li, C. Won, H. F. Ding, Z. Q. Qiu, and Y. Z. Wu, *Phys. Rev. B* **91**, 134428 (2015).
- [43] J. Li, A. Tan, S. Ma, R. F. Yang, E. Arenholz, C. Hwang, and Z. Q. Qiu, *Phys. Rev. Lett.* **113**, 147207 (2014).
- [44] Q. Li, M. Yang, A. T. N'Diaye, C. Klewe, P. Shafer, N. Gao, T. Y. Wang, E. Arenholz, X. Zhang, C. Hwang, J. Li, and Z. Q. Qiu, *Phys. Rev. Mater.* **3**, 114415 (2019).
- [45] J. Wu, J. S. Park, W. Kim, E. Arenholz, M. Liberati, A. Scholl, Y. Z. Wu, C. Hwang, and Z. Q. Qiu, *Phys. Rev. Lett.* **104**, 217204 (2010).
- [46] J. Zhu, Q. Li, J. X. Li, Z. Ding, C. Y. Hua, M. J. Huang, H.-J. Lin, Z. Hu, C. Won, and Y. Z. Wu, *J. Appl. Phys.* **115**, 193903 (2014).
- [47] J. Zhu, Q. Li, J. X. Li, Z. Ding, J. H. Liang, X. Xiao, Y. M. Luo, C. Y. Hua, H.-J. Lin, T. W. Pi, Z. Hu, C. Won, and Y. Z. Wu, *Phys. Rev. B* **90**, 054403 (2014).
- [48] X. Tao, Q. Liu, B. Miao, R. Yu, Z. Feng, L. Sun, B. You, J. Du, K. Chen, S. Zhang, L. Zhang, Z. Yuan, D. Wu, and H. Ding, *Sci. Adv.* **4**, eaat1670 (2018).